文章编号：1001－9014(2018)01－0001－07

DOI:10.11972/j.issn.1001－9014.2018.01.001

The study of using infrared thermal image to assist surgery of coronary artery bypass

CHANG Chia-Jui[1*], TSAI Chien-Sung[2], TANG Shiang-Feng[3], YANG Chi-Shih[4], LIN Wen-Jen[3], LIU Chiang-Lung[1], CHEN Tzu-Chiang[1]

(1. Defense Science, Chung Cheng Institute of Technology National Defense University, Taiwan Taoyuan 33550, China;
2. National Defense Medical Center, Department of Surgery, Taiwan Taipei 11490, China;
3. Materials & Electro-Optics Research Division, National Chung Shun Institute of Technology, Taiwan Taoyuan 32599, China;
4. Lee-Ming Institute of Technology, Department of Mechanical Engineering, Taiwan New Taipei 24346, China)

Abstract: Digital infrared thermography is suitable for monitoring the planar two-dimensional temperature distribution of curved surfaces of objects by sensing their infrared radiation. Cardiac infrared thermography also has a thermal coronary angiography alias. This study proposes a digital image processing methodology for locating blood clot blockage. This methodology contains four consequent processes. The two-dimensional gray scale infrared thermograph pixels are first binarized and classified as background or coronary arteries using multi-thresh adaptive segmentation. The coronary artery contours are extracted from segmented raw pixels using continuous pepper-like pixel removal, erosion, subtraction, recursive neighborhood visiting, contour point-list construction and short edge deletion. In the third process one coronary artery branch is selected by physicians for calculating the longest curved central axis using morphological thinning and neighborhood analysis. In the last process the nearest left and right distances from each pixel along the directional central axis to its corresponding boundary contour are added as the coronary artery variable diameter at the current pixel's position. A variable diameter versus straighten length diagram along this axial curved path is plotted to provide useful physiological information to the physician. An obstruction rate equation is then defined to calculate the possible vascular blockage positions with the local minimal rates. Finally, preoperative cases are tested to prove the predictive positions are correct in comparison to individual patient myocardial perfusion imaging.

Key words: infrared thermal thermograph, thermal coronary angiography, coronary artery bypass surgery, variable diameter, obstruction rate

PACS: 07.20.-n, 42.30.Va

Introduction

Coronary artery disease always occurs in adults when blood cholesterol is deposited onto the inner arterial walls[1]. Atherosclerosis brings about deposited cholesterol plaque that makes it easier for blood clots to block the blood flow[2]. Due to the poor blood flow supply, the healthy cardiac muscle gradually succumbs to necrosis. A heart attack allows the patient to feel several symptoms; chest pains and discomfort or pain in the back. Sometimes the patient's condition prevents the application of angioplasty (PTCA), stents, or causes such application to be ineffective[3]. The final resort is applying CABS to the predilection vessel such as the right coronary artery (RCA), left anterior descending artery (LAD), left circumflex artery (LCX) or obtuse marginal artery (OM)[4].

According to the medical intervention time sequence, there are three appropriate opportunities to implement anastomosis thermography after the CABS thoracotomy[5]. Preoperative, intraoperative and postoperative infrared thermograph evaluations may be performed to immediately inform surgeons about vascular conditions. At the preoperative evaluation stage, before the saphenous vein (SVG) or internal thoracic artery (ITA) are grafted downstream of the vascular blockage, infrared thermographs can provide suitable grafting position suggestions to supply additional blood flow[6]. At the middle intraoperative evaluation stage, surgeons may use thermography to judge whether a blood leakage or bottleneck is formed during the perfusion pressure test just after the anastomo-

Received date: 2017-01-25, **revised date**: 2017-08-23　　收稿日期:2017-01-25, 修回日期:2017-08-23

Biography: CHANG Chia-Jui (1972-), male, Taiwan, China. Ph. D. candidate, Research fields focus on infrared thermal image processing and power electronics design. E-mail: j88eric@gmail.com

* **Corresponding author**: E-mail: j88eric@gmail.com

sis[7-13]. At the third postoperative evaluation stage, vascular blockage section thermographs can provide surgeons with valuable information on the improved level of arterial patency.

All objects in the universe emit infrared radiation with temperatures greater than absolute zero. Wien's displacement law states that the peak thermal radiation wavelength of any object is inversely proportional to its absolute temperature with Wien's displacement constant b ($\lambda \max T = b$, where $b = 2.897\,772\,1 \times 10^{-3}$ mK)[14]. Assume that the human body skin to trunk core temperature variation range is 33.2 to 38.2℃[15], the infrared radiation wavelength emitted from the human body should be between 9.464 and 9.312 μm according to Wien's displacement law. A thermal imaging camera (Thermoteknix Systems Ltd, Model no. Miracle 110K, United Kingdom) 384 × 288 pixels with 8 ~ 12 μm spectral range was used for medical inspection purposes to ensure that the thermo graphic output was fine and clear.

Many good investigations regarding thermal coronary angiography have been published with successful clinical applications. In 1989 Mohr observed the blood flow condition after an anastomosis operation. Due to obstructing cardiovascular imaging by fat and myocardial tissue, saline perfusion was applied with a 4 degree temperature difference. The final result proved that the angiographies image quality was enhanced while either SVG bypassed to OM or IMA bypassed to LAD[7]. In 1991 Mohr released a hemostat after LAD bypass anastomosis to generate a temperature difference between blood flow (30 to 36 degrees) and the heart surface (ambient temperature 25.5 degrees) to strengthen the angiographies contrast[6]. In 1997, Falk[8] and van Son[9] used cold saline to cool the heart surface and then released a LAD hemostat to generate a temperature difference between warm blood and the cooled heart surface. Better image quality was thereby obtained after saline cooling. In 2000 Suma observed the anastomosis quality between ITA and LAD with the assistance of a CO_2 cooler to find a stitching failure. The anastomosis condition was evaluated objectively and the failure was found by ischemia downstream and finally corrected[10]. In 2003, Sonmez[10] alternatively injected cold and warm saline to strengthen contrast. The cold saline was first injected into the SVG or ITA graft to cool the coronary artery or the heart. Warm saline or warm blood was then injected into the graft to highlight the coronary artery in thermograph. Cold saline was changed back to eliminate the coronary artery hotspot within a very short time. If parts of the distal or proximal artery did not disappear, the anastomosis was then a failure[11]. In 2007 Iwahashi used an infrared thermal camera in a coaxial manner with a visible light CCD using cold saline injection (30°C, 3 ~5ml) and then releasing the hemostat (5 seconds) to determine the vascular circulation. If the circulation was bad, the bypass graft end was rebuilt. Iwahashi also found that sometimes the fat was too thick to obtain clear images[12].

Although previous studies prove that the thermal coronary angiography really works as an auxiliary instrument, the vast majority of investigators still utilize subjective evaluation. This subjective evaluation is extremely affected by human interference, the physician's experience or judgment ability resulting in different clinical reasoning. This study proposes a novel digital image processing methodology to suggest possible vascular blockage positions for CABS. The proposed methodology contains four primary stages: multi-thresh adaptive coronary angiography segmentation, coronary artery contour extraction, curved central axis morphological analysis and coronary artery variable diameter calculation. An obstruction rate equation is adopted to locate the possible blockage with a local minimal rate.

1 Multi-threshold adaptive segmentation of coronary angiography

At the beginning of angiography analysis the coronary artery regional range must be classified first. As the grayscale image in Fig. 1 shows, the hot-spots pattern is usually complex because there are several interference factors involved to classifying thermograph pixels as background or coronary artery, such as the thoracotomy opening boundary, surgical instruments, drainage tubes, gauze, stitches, local cardiac muscle hot spots, fat tissue, pericardium and the restricted field of view (FOV).

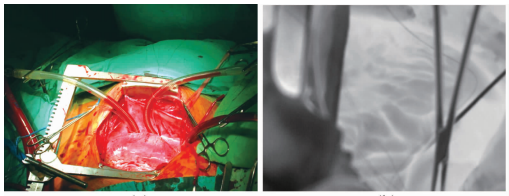

(a) (b)

Fig. 1 (a) The complex surgical environment and (b) The angiography complex hot-spots pattern

1.1 Filter mask by angiography

As the original angiography in Fig. 2 shows, the instruments are removed as much as possible, the focal length is adjusted as close as possible and the coronary artery view field is aimed as central as possible. After taking a suitable angiography, two multi-thresh adaptive segmentation steps are applied. The first image preprocessing step contains histogram equalization[16] and low-pass processing. The histogram equalization redistributes the order of gray levels using a probability density function, so that the new distribution strengthens the blood vessel details, as shown in Fig. 3. A 3-by-3 low-pass filter mask with a coefficient valued of 1/9 is then applied to average the thermography noise. The sample low-pass filtered angiography is shown in Fig. 4.

1.2 The Otsu method

The second multi-threshold adaptive segmentation step uses a statistical method with a variable square mask size to determine whether the central pixel belongs to coronary artery or not. The variable square mask size starts from 3 pixels and stops at any larger odd number with a maximal standard deviation. Assume that the central pixel position is centered; one half of the mask size is the radius. Only the pixels in the circular range are taken into consideration for the statistical calculation. In Eqs. 1-2, N is the number of pixels in the circular range, G_i is the gray level of pixel i, μ_{max} is the average gray level in

Fig. 2　The original input angiography

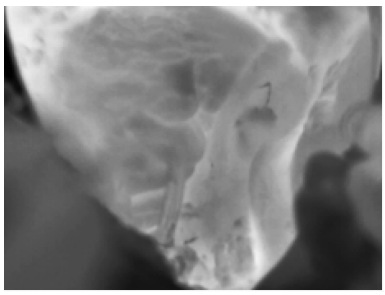

Fig. 3　The histogram equalized angiography

Fig. 4　The 3 × 3 low-pass filtered angiography

the circular range with the maximal standard deviation $\sigma_{\max}$. In Eqs. 3-4, ΔA_i is the unit one area of any pixel, A and B is the number of pixels with gray levels greater than or smaller than $\mu_{\max}$. Equation 5 shows the compensation Equation for threshold T_i for an uneven distribution within the circular range, as shown in Fig. 5. The final step binarizes a specific gray pixel and classifies it into the background or coronary artery group, as shown in Eq. 6.

$$\mu_{\max} = \frac{\sum_N G_i}{N} \quad , \quad (1)$$

$$\sigma_{\max} = \sqrt{\frac{\sum_N (G_i - \mu)^2}{N}} \quad , \quad (2)$$

$$A = \sum_N \Delta A_i (\text{if } G_i > \mu_{\max}) \quad , \quad (3)$$

$$B = \sum_N \Delta A_i (\text{if } G_i < \mu_{\max}) \quad , \quad (4)$$

$$\begin{cases} T_i = \mu_{\max} - \sigma_{\max} \dfrac{B}{N} (\text{if } A > B) \\ T_i = \mu_{\max} + \sigma_{\max} \dfrac{A}{N} (\text{if } A < B) \end{cases} \quad , \quad (5)$$

$$\begin{cases} B_i = 1, \text{coronary artery } (\text{if } G_i > T_i) \\ B_i = 0, \text{ background} (\text{if } G_i < T_i) \end{cases} \quad , \quad (6)$$

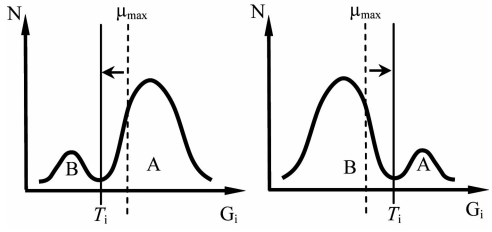

Fig. 5　The compensation from average gray level toward the threshold

Fig. 6　Otsu binarized angiography using (a) single threshold and (b) multi-threshold

Figures 6(a) and 6(b) show two binarized results to compare the Otsu method performance[17] using a single threshold for all pixels and multi-threshold for individual pixels. The Otsu method can only identify the heart region. We propose and adaptive method that uses infrared thermal images which can identify the heart profile and also the detailed coronary artery pattern.

2　Coronary artery contours extraction

After the segmented raw pixels are classified in the segmentation process, six extraction process steps are applied to generate contour point-lists, including continuous pepper-like pixel removal, erosion, subtraction, recursive contour neighborhood visiting, point linked-list integration and short edges deletion. At the beginning lots of pepper-like pixels are spread among the coronary arteries. Some redundant data in the segmented raw pixels, which may be cardiac muscle or thoracotomy opening pixels, are continuously removed by a binary averaging convolution. This convolution uses a 3-by-3 mask with nine coefficients valued 1/9. The binary value of a foreground pixel is 1 and that of a background pixel is 0. If the convolution result exceeds 0.5, the central pixel is reserved otherwise the central pixel is removed. The new pixel-removed angiography is compared pixel by pixel with the original one. If the state of any pixel is changed, the next averaging convolution is applied on the new angiography until nothing is changed, as shown in Fig. 7.

The second step erodes the binary coronary artery one time and shrinks internally with a width of one pixel. The original coronary artery is then subtracted using erosive angiography pixel by pixel to generate the coronary artery contours, as shown in Fig. 8. If an original foreground pixel encounters an eroded background pixel, the subtracted pixel is considered as foreground and a point

Fig. 7 The pepper-like pixels are removed continuously

Fig. 8 The angiography contours after erosion and subtraction

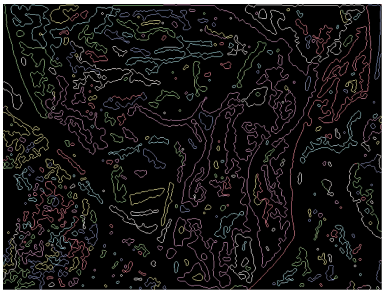

Fig. 9 The angiography colored by recursive contour neighborhood visiting

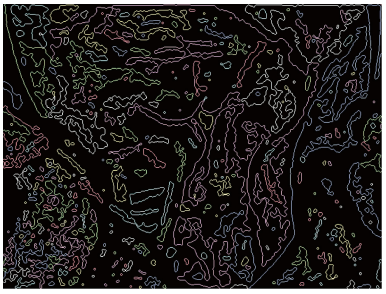

Fig. 10 The angiography integrated by linked-list

Fig. 11 The angiography that short edges are deleted

linked-list is constructed. Otherwise, the other three conditions generate a background subtracted pixels. The fourth step is searching for any subtracted foreground pixels in the angiography from left to right and top to bottom. If any contour pixel is found, the corresponding position is also labeled by a two-dimensional Boolean array. The found pixel is soon followed by an 8-neighborhood recursive connection searching and the connected pixels are also labeled. Each non-stopping visited pixel is recorded consequently into the same point linked-list. Because there may be some point linked-lists belonging to a single loop of a vessel contour, the fifth step integrates all of the connected linked-lists into a single list. There are nested double loops to test whether two different linked-lists are geometrically connected. If any one pair of linked-lists is found, four connection situations are checked with head-to-head, head-to-tail, tail-to-head and tail-to-tail methods. Any reverse point linked-list order is applied if needed for a single directional connection. After integrating all point linked-lists, a minimal pixel number is set and any point linked-list shorter than a preset number is deleted at the last step. The final recursive visiting, point integration and short edges deletion results are shown in Figs. 9-11, respectively.

3 Curved central axis morphological analysis

The next process is computing the longest curved central axis for the next process to measure the diameters along it. Five morphological and neighborhood analysis steps are introduced in this process, including skeleton thinning, neighborhood labeling, adjacent trident points deletion, false trident points deletion and continuous shorter branch pruning. In this process surgeons can select any one of the branch contours in the angiography on site. Figure 12 shows a smaller branch demonstrated for simple morphological analysis illustration.

At the skeleton thinning step four horizontal/vertical look-up table, thinning[18], cross-mask[19] and X-fork mask[20] skeleton rules are taken into consideration and tested individually. The morphological erosion operation is performed continuously using a hit-and-miss transform structural element (i. e. the central pixel is erasable if the pattern matches)[21]. The horizontal/vertical look-up table method (LUT, $2^8 = 256$ masks) is selected in this study for the continuous curved central axis connectivity.

At the neighborhood labeling step the connected neighborhood of each skeleton pixel is inspected and colored. The integer skeleton pixel label may vary from 1 to 8. The pixels at the skeleton end with one neighborhood are colored dark green. The pixels in the middle of the skeleton curve with two neighborhoods are colored blue. The pixels on trident points with three or more neighbor-

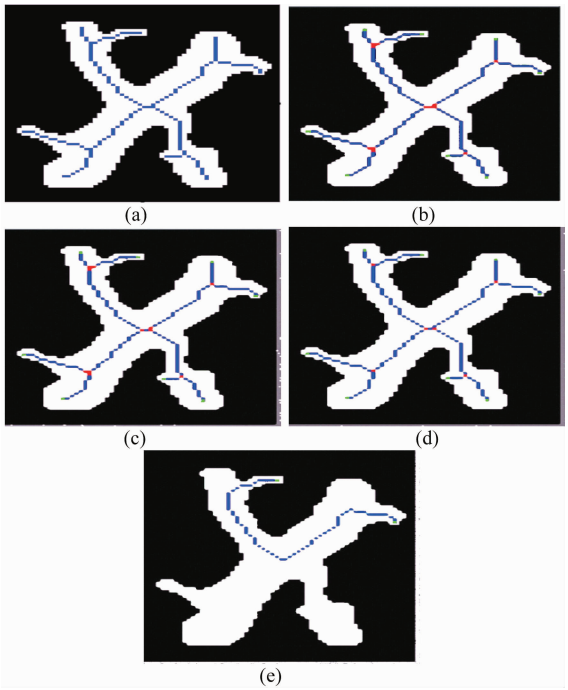

Fig. 12　Five morphological analysis steps for the curved central axis. (a) Skeleton thinning, (b) neighborhood labeling (red: trident points, green: end points), (c) adjacent trident point deletion, (d) false trident point deletion, (e) continuous pruning of shorter branches

hoods are colored red. The label number and pixel color provide the needed information to prune the shorter branches and leave the longest branch.

To maintain exactly one pixel located at a trident position, two kinds of deletion (i. e. by changing the label from 3 to 2 and change the color from red to blue) are used for adjacent trident and false trident points. These two operations ensure that there are no trident points clustered together for the next pruning step.

At the continuous shorter branch pruning step, any two end pixels in dark green color are selected for tracing the skeleton and counting the number of neighborhoods pixel by pixel. This tracing stops when the other new trident pixel in red color or the end pixel in dark green color is visited. Then two counting numbers of different branches are compared and the shorter one is pruned. The pruned trident pixel is kept and its color is also changed from red to blue with a label of two neighborhoods.

5　Variable diameter calculation of coronary artery

The fourth process attempts to compute different coronary artery diameters along the curved central axis. This process includes three steps; tangent line computation, nearest contour point search and variable diameter plotting diagram versus straighten length, as shown in Fig. 13. For a given curved central axis, the coronary artery diameter is defined by the shortest distance from the blood vessel right to left wall and perpendicular to the central axis. Based on the perpendicular diameter, the tangent directions at each curved central axis pixel should be computed first in order to obtain the radial directions.

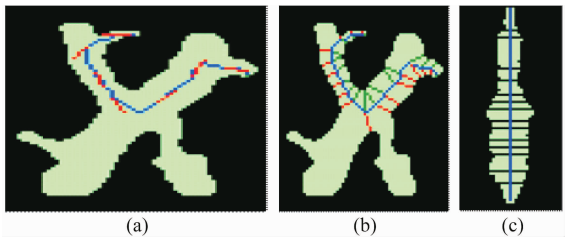

Fig. 13　Three variable diameter coronary artery calculation steps: (a) tangent line computation, (b) nearest contour point search and (c) variable diameter versus straighten length plot diagram

This study proposed a useful distance inverse weighting formula instead of the least square Equation. The tangent line of the least square equation assumes that every pixel of the curved central axis has the same weight. The generated slope is the global average of all local tangent line slopes. On the other hand, the proposed distance inverse weighting tangent line is more precisely tangent to the target pixel on the central axis with a larger weight for its adjacent neighbor pixels, as shown in Fig. 14.

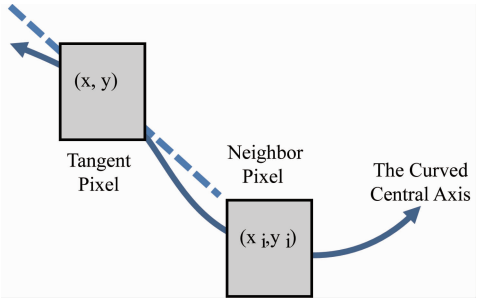

Fig. 14　The curved central axis tangent line

$$S_i = (y_i - y):(x_i - x) = \Delta y_i:\Delta x_i = \frac{\Delta y_i}{\sqrt{\Delta x_i^2 + \Delta y_i^2}}:\frac{\Delta x_i}{\sqrt{\Delta x_i^2 + \Delta y_i^2}} = \frac{\Delta y_i}{L_i}:\frac{\Delta x_i}{L_i}, \quad (7)$$

$$W_i = \frac{\frac{1}{L_i}}{\cdots + \frac{1}{L_{i-1}} + \frac{1}{L_i} + \frac{1}{L_{i+1}}}, \quad (8)$$

$$s = \sum w_i \Delta y_i : \sum w_i \Delta x_i, \quad (9)$$

The individual slope S_i of the local tangent line is first computed for each neighbor pixel (x_i, y_i) with respect to the tangent pixel (x, y), as shown in Eq. 7. Equation 8 illustrates how to compute the individual weights of the neighbor pixels within a symmetric pixel span. If the tangent pixel is near the central axis end, only the effective neighbor pixels are taken into consideration. Equation 9 integrates several local tangent slopes to obtain a global weighted slope S. The perpendicular diameter slope in the radial direction can then be computed using $-1/S$, with the tangent point coordinate (x, y) and the radial line Equation can then be obtained.

In the second nearest contour point search step all

branch contour pixels are checked to identify the two nearest contour points using two tangent line and radial straight line equation. The tangent line Equation can classify which side (i.e. the left side and right side) along the directional central axis, and the radial line equation can select the two nearest contour pixels. In Eqs. 10-13, a straight length L of the curved central axis is first computed by summing the number of 4-neighborhoods as 1, and the diagonal-neighborhoods as $\sqrt{2}$. The diameter $D(x)$ can then be obtained by adding the right $R_{\text{Right}}(x)$ and left radii $R_{\text{Left}}(x)$ at the position x. The average radius is obtained by summing all local radii and dividing by the straight length. Finally, the obstruction rate $\delta_{\text{Neck}}(x)$ is defined by the diameter difference divided by the average diameter.

$$D(x) = R_{\text{Right}}(x) + R_{\text{Left}}(x), x \in [0, L] \quad (10)$$

$$\begin{cases} R_{\text{Right Average}} = \dfrac{\int_0^L R_{\text{Right}}(x)\,dx}{L} = \dfrac{\sum_1^L R_{\text{Right}}(x)}{L} \\ R_{\text{Left Average}} = \dfrac{\int_0^L R_{\text{Left}}(x)\,dx}{L} = \dfrac{\sum_1^L R_{\text{Left}}(x)}{L} \end{cases} \quad (11)$$

$$D_{\text{Average}} = R_{\text{Right Average}} + R_{\text{Left Average}} \quad (12)$$

$$\delta_{\text{Neck}}(x) = \frac{D(x) - D_{\text{Average}}}{D_{\text{Average}}} = \frac{[R_{\text{Right}}(x) - R_{\text{Right Average}}] + [R_{\text{Left}}(x) - R_{\text{Left Average}}]}{R_{\text{Right Average}} + R_{\text{Left Average}}} \quad (13)$$

6 Results and discussion

After the coronary artery variable diameter calculation step, the varying diameters of each pixel along the curved central axis are obtained by adding the left and right radii. Every paired left and right radius is the distance from that central axis pixel to the nearest left-side and right-side vessel contour. These varying diameters are plotted in the middle diagram of Fig. 15 to show the variable diameter versus straighten length. For average diameter calculation, the local diameters along the curved central axis between two trident points (or one trident point and one end point) are summed. The final average diameter can then be obtained for a specific branch vessel.

The testing environment is implemented using a thermal imaging camera (Thermoteknix, Miricle 110 K, 384 ×288 pixels, 8 ~ 12 μm) set at the Tri-Service General Hospital to collect the clinical data. The computer aided obstruction rate analysis software was developed in Borland C + + Builder 6.0 on a TOSHIBA Satellite core i5 notebook. The clinical analysis result is shown in Fig. 15. The left diagram is the image processing area; the middle diagram is the variable diameter versus straightened length with three marked thrombosis positions. The right diagram plots the variable obstruction rate along the straightened central axis with three local minimal values of −83.4%, −28.7% and −66.8%.

According to the journal paper entitled "Cross-sectional area coronary arteries measurement using CT angiography at the bifurcation level: is there a relationship?"[22], Samet describes the statistical diameter analysis of three vessels LMCA, LAD, and CX using cardiovascular CT images. A geometric relationship with LMCA = 3.870 + 0.718 · LAD + 0.434 · CX is chosen as the golden geometric relationship rule in this paper to verify the correct automatic software pipeline measurement method. In the first thermal image test shown in Fig. 16, the theoretical value of the LMCA golden rule and the automatically measured software values are 12.9 mm and 6.4 mm = R_L3.3 + R_R3.1, respectively. There is only a little difference with 0.77% (thermal image scale 2:1). With similar consistency in the second test thermal image shown in Fig. 17, the theoretical and measured values are 13.4mm and 6.5 mm = R_L3.2 + R_R3.3 respectively. There is a small difference of 2.9% (thermal image scale 2:1).

With the verified results for Samet's Golden Rule using the above two testing thermal images, the three diameters measured in this research showed no excessive difference between the infrared and CT. This represents that less expensive infrared thermography can indeed replace the expensive CT equipment in practical clinical applications. The infrared pipeline measurement method proposed by this paper can obtain the necessary coronary artery diameter clinical information cheaper, faster and easier during on-site thoracic surgery. This proves that the proposed pipeline measuring method is both convenient and progressive.

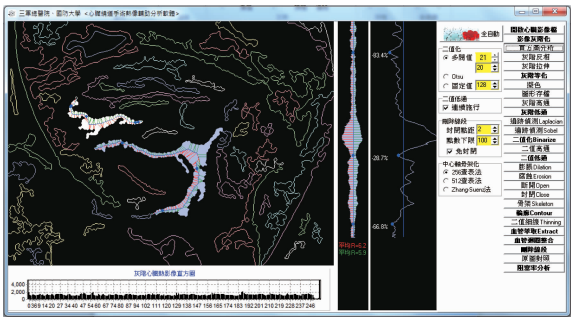

Fig. 15 The computer aided obstruction rate analysis software

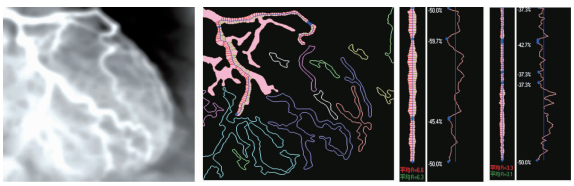

Fig. 16 Analysis Rule in the first test thermal image (CX = 12.9 mm, LAD = 6.4 mm)

7 Conclusions

A computer aided obstruction rate analysis method was proposed in this study to assist surgeons with dynamic blood flow information using thermal coronary angiography. A digital image processing methodology is proposed

Fig. 17　Analysis Rule in the first test thermal image (CX = 13.4 mm, LAD = 6.5 mm)

to locate the cardiovascular thrombosis bottleneck. Clinical testing shows the proposed four processes (multi-thresh adaptive coronary angiography segmentation, coronary artery contour extraction, curved central axis morphological analysis and coronary artery variable diameter calculation) can successfully locate the possible local minimal obstruction rate positions. It was also proven that the proposed method can dynamically provide real-time critical cardiovascular physiological information for clinical surgeons.

Acknowledgement

The authors would like to thank the financial support of this research under grant No. 103-2218-E-234-001. The authors also thank the Tri-Service General Hospital and Chung Cheng Institute of Technology for the clinical assistance.

References

[1] L. Aschoff. Observations Concerning the Relationship between Cholesterol Metabolism and Vascular Disease [J]. *Br Med J*, 1932, **2**(12): 1131 - 1134.

[2] L. Dintenfass. Blood Rheology in Pathogenesis of the Coronary Heart Diseases [J]. *American Heart Journal*, 1969, **7**(1), 139 - 147.

[3] C. E. Buller, Vladimir Dzavik, Ronald G. Carere, et al. Primary Stenting versus Balloon Angioplasty in Occluded Coronary Arteries [J]. *Circulation*, 1999, **100**: 236 - 242.

[4] W. C. Little, Martin Constantinescu, Robert J, et al. Can Coronary Angiography Predict the site of a Subsequent Myocardial Infarction in Patients with mild-to-moderate Coronary Artery Disease [J]. *Circulation*, 1988, **78**(11). 1157 - 1166.

[5] Donald B. Doty and John R. Doty. *Cardiac Surgery: Operative Technique*, 2nd ed [B]. Saunders: Elsevier, 2012.

[6] F. W. Mohr, V. Falk, H. Krieger, et al. IMA-Graft Patency Control by Thermal Coronary Angiography during Coronary Bypass Surgery [J]. *European Journal of Cardi,o Thoracic Surgery*, 1991, **5**: 534 - 541.

[7] F. W. Mohr, Jack Matloff, Warren Grundfest, et al. Thermal Coronary Angiography: A Method for Assessing Graft Patency and Coronary Anatomy in Coronary Bypass Surgery [J]. *The Annals of Thoracic Surgery*, 1989, **47**: 441 - 449.

[8] V. Falk, Anno Diegeler, Thomas Walther, *et al.* Intraoperative Patency Control of Arterial Grafts in Minimally Invasive Coronary Artery Bypass Graft Operations by Means of Endoscopic Thermal Coronary Angiography [J]. *The Journal of Thoracic and Cardiovascular Surgery*, 1997, **114**(3): 507 - 509.

[9] J. A. M. van Son, Volkmar Falk, Thomas Walther, *et al.* Thermal Coronary Angiography for Intraoperative Testing of Coronary Patency in Congenital Heart Defects [J]. *The Annals of Thoracic Surgery*, 1997, **64**: 1499 - 1500.

[10] H. Suma, T. Isomura, T. Horii, *et al.* Intraoperative Coronary Artery Imaging with Infrared Camera in Off-Pump CABG [J]. *The Annals of Thoracic Surgery*, 2000, **70**: 1741 - 1742.

[11] B. Sonmez, H. Arbatli, S. Tansal, *et al.* Real-Time Patency Control with Thermal Coronary Angiography in 1401 Coronary Artery Bypass Grafting Patients [J]. *European Journal of Cardio-thoracic Surgery*, 2003, **24**: 961 - 963.

[12] H. Iwahashi, T. Tashiro, N. Morishige, *et al.* New Method of Thermal Coronary Angiography for Intraoperative Patency Control in Off-Pump and On-Pump Coronary Artery Bypass Grafting [J]. *The Annals of Thoracic Surgery*, 2007, **84**: 1504 - 1507.

[13] T. Handa, Rajesh G. Katare, S. Sasaguri, *et al.* Preliminary Experience for the Evaluation of the Intraoperative Graft Patency with Real Color Charge-Coupled Device Camera System: An Advanced Device for Simultaneous Capturing of Color and Near-Infrared Images During Coronary Artery Bypass Graft [J]. *Interactive Cardio Vascular and Thoracic Surgery*, 2009, **9**: 150 - 154.

[14] A. I. Fisenko, S. N. Ivashov. Determination of the True Temperature of Emitted Radiation Bodies from Generalized Wien's Displacement Law [J]. *Journal of Physics D: Applied Physics*, 1999, **32**(11), No. 22.

[15] M. Sund-Levander, C. Forsberg, L. K. Wahren, et al. Normal oral, rectal, tympanic and axillary body temperature in adult men and women: a systematic literature review [J]. *Scand J Caring Sci*, 2002, **16**(2): 122 - 8.

[16] J. A. Stark, Adaptive image contrast enhancement using generalizations of histogram equalization [J]. *IEEE Transactions on Image Processing*, 2000, **9**(5): 889 - 896.

[17] R. C. Gonzalez, R. E. Woods. *Digital Image Processing*, 2_nd ed [B]. New Jersey: Prentice Hall, 2001, ch. 10.

[18] T. Y. Zhang, C. Y. SUEN. A Fast Parallel Algorithm for Thinning Digital Patterns [J]. *Comm ACM*, 1984, **27**(3): 236 - 239.

[19] S. Chen, H. RM. Recursive Erosion, Dilation, Opening, and Closing Transforms [J]. *IEEE Transactions on Image Processing*, Mar. 1995, **4**(3).

[20] R. C. Gonzalez, R. E. Woods. *Digital Image Processing*, 2_nd ed [B]. Prentice Hall, 2002, ch. 9.

[21] M. Ahmed, R. Ward. A Rotation Invariant Rule-Based Thinning Algorithm for Character Recognition [J]. *IEEE Transactions on Pattern Analysis and Machine Intelligence*, 2002, **24**(12).

[22] S. Verim, E. Öztürk, U. Küçük *et al.* Cross-sectional area measurement of the coronary arteries using CT angiography at the level of the bifurcation: is there a relationship [J]. *Cross-sectional area measurement of the coronary arteries on CT angiography*, 2015, 21(6): 455 - 458.